Biomimetic Virtual Constraint Control of a Transfemoral Powered Prosthetic Leg

Robert D. Gregg and Jonathon W. Sensinger

Abstract— **This paper presents a novel control strategy for a powered knee-ankle prosthesis based on biomimetic virtual constraints. We begin by deriving kinematic constraints for the "effective shape" of the human leg during locomotion. This shape characterizes ankle and knee motion as a function of the Center of Pressure (COP)—the point on the foot sole where the ground reaction force is imparted. Since the COP moves monotonically from heel to toe during steady walking, we adopt the COP as the phase variable of an autonomous feedback controller. We show that our kinematic constraints can be enforced virtually by an output linearizing controller that uses only feedback available to sensors onboard a prosthetic leg. This controller produces walking gaits with human-like knee flexion in simulations of a 6-link biped with feet. Hence, both knee and ankle control can be coordinated by one simple control objective: maintaining a constant-curvature effective shape.**

I. Introduction

High-performance prostheses could significantly improve the quality of life for lower-limb amputees, whose ambulation is typically slower, less stable, and less efficient than able-bodied persons [1], [2]. The recent advent of mechanically powered legs (e.g., [3]–[5]) presents new opportunities in prosthetic control systems, but many control challenges currently limit their clinical viability.

The prevailing methodology independently controls each joint and each phase of the gait cycle, requiring clinicians to spend a significant amount of time tuning each controller to the individual. For example, the Vanderbilt leg [3] changes proportional-derivative (PD) gains for the ankle and knee according to five discrete phases. The iWalk ankle [4] also uses a finite state machine but trades the simplicity of PD controllers for the biomimetic behavior of muscle reflex models. Reliable tuning of these increasingly complex control strategies is of paramount importance to lower-limb amputees, who experience frequent falls [1].

These challenges could potentially be addressed by parameterizing a nonlinear control model with a mechanical representation of the gait cycle phase, which could be continuously sensed by a prosthesis to match the body's progression through the cycle. Feedback controllers for *autonomous walking robots* have been developed that "virtually" enforce kinematic constraints [6]–[8], which define desired joint patterns as functions of a mechanical phase variable (e.g., the stance leg angle). This nonlinear control framework, known as output linearization, has proven successful in experimental bipedal robots such as RABBIT [6], ERNIE [6], and MABEL [7] but has never been applied to the field of prosthetics. This approach could be dovetailed with biologically-inspired constraints to make prosthetic legs more robust and easily tuned than controllers used to date.

For this purpose we examine studies suggesting that human locomotor patterns depend on the progression of the Center of Pressure (COP)—the point on the foot sole where the resultant ground reaction force is imparted. Hansen et al. showed that during human walking, geometric relationships exist between stance leg joints and the COP [9]–[12]. When the COP trajectory is examined relative to the shank, it is found that the ankle and foot together conform to a circular rocker shape (coined "effective shape") that is invariant over walking speeds, heel heights, and body weights. The fact that the COP moves monotonically from heel to toe during steady gait [13] suggests that the COP can serve as the phase variable of a virtual constraint. However, without the availability of state feedback from the coupled human body, it is unclear how a prosthetic control system can linearize its output dynamics to enforce a virtual constraint.

We recently derived such a controller for a prosthetic ankle based on the ankle-foot (AF) effective shape [14], but this strategy did not include the knee joint. Fortunately the knee-ankle-foot (KAF) effective shape—the COP trajectory in a thigh-based reference frame—has approximately the same curvature as the AF shape during walking [10], suggesting that the KAF shape can serve as a second virtual constraint.

This paper shows that knee and ankle control during walking can be coordinated by one simple objective: maintaining a constant curvature in the effective shapes. This work is clinically significant to the ease of use and reliability of powered prosthetic legs. The technical contributions of the paper are two-fold: (i) we show that the effective shapes between the COP, ankle, and knee correspond to two kinematic constraints, which (ii) can be simultaneously enforced as virtual constraints by an output linearizing controller *using feedback available to sensors onboard a prosthetic leg*. This includes a generalization of the output linearization framework from [14]—which is subject to external forces and holonomic constraints—to the case of vector outputs. The resulting control strategy drives ankle and knee patterns as a function of the COP, a novel choice of phase variable that unifies the entire single-support cycle.

Asterisk indicates corresponding author.

R.D. Gregg* is with the Departments of Mechanical Engineering and Bioengineering, University of Texas at Dallas, Richardson, TX 75080.

J.W. Sensinger is with the Center for Bionic Medicine, Rehabilitation Institute of Chicago and the Departments of Physical Medicine & Rehabilitation and Mechanical Engineering, Northwestern University, Chicago, IL 60611. {rgregg,sensinger}@ieee.org

Robert De Moss Gregg, IV, Ph.D., holds a Career Award at the Scientific Interface from the Burroughs Wellcome Fund. This research was also supported by USAMRAA grant W81XWH-09-2-0020.

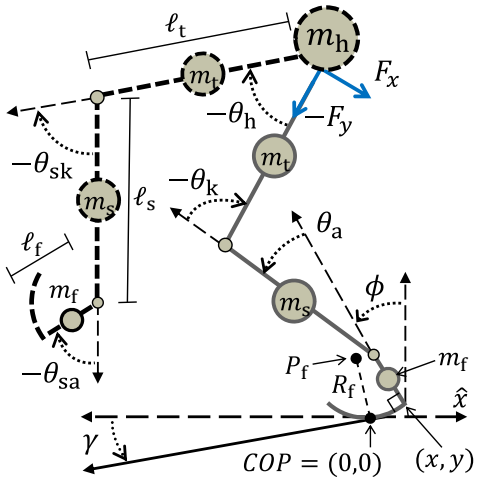

Fig. 1. Biped model showing the prosthetic stance leg in solid gray and the body in dashed black. Positive/negative movement are respectively termed dorsiflexion/plantarflexion for the ankle and extension/flexion for the knee.

We demonstrate this approach by simulating a biped model and find stable gaits with human-like knee flexion.

II. Leg Model

In this paper we use a planar 6-link biped model to design the prosthesis controller and to simulate walking. The biped of Fig. 1 has a hip joint, knees, and ankles with constant-curvature rocker feet to approximate the deformation of human feet during walking [15]. We consider the stance leg (shown in solid gray) to be a prosthesis, which connects to the body (shown in dashed black) at the hip. We will separately model the prosthetic leg for our control derivation in Section III and return to the full biped model for the purpose of simulation in Section IV. We model the prosthetic leg as a kinematic chain with respect to a global reference frame defined at the COP during stance. We then derive a holonomic constraint that forces the COP to move along the rocker foot in the continuous dynamics. Note that this constraint is different than the effective shape, which depends on both the foot curvature and joint motion (Section III). We conclude the current section by discussing the swing period.

Dynamics. The configuration of the leg is given by $q = (x, y, \phi, \theta_a, \theta_k)^T$, where x, y are the Cartesian coordinates of the heel, ϕ is the foot orientation with respect to vertical, θ_a is the ankle angle, and θ_k is the knee angle. The state of the dynamical system is given by vector $z = (q^T, \dot{q}^T)^T$, where $\dot{q}$ contains the joint velocities. The state trajectory evolves according to a differential equation of the form

$$M(q)\ddot{q} + C(q,\dot{q})\dot{q} + N(q) + A^T(q)\lambda \quad = \quad \tau \qquad (1)$$

where M is the inertia/mass matrix, C is the matrix of Coriolis/centrifugal terms, N is the vector of gravitational forces, A is the constraint vector for the rocker foot (modeling foot compliance), and λ is the Lagrange multiplier consisting of physical forces from the foot constraint. The external forces $\tau = Bu + J^T(q)F$ are comprised of actuator torques and interaction forces with the body, respectively.

Ankle and knee actuation is provided by torque input u and mapped into the leg's coordinate system by $B = (0_{2\times 3}, I_{2\times 2})^T$. The interaction force $F \in \mathbb{R}^3$ at the socket—the connection between the prosthesis and body at the hip in Fig. 1—is composed of linear forces in the plane and the moment about the normal axis. Force vector F, which acts at the end-point of the leg's kinematic chain, is mapped to torques and forces at the leg joints by the *body Jacobian* matrix $J(q)$ [16]. The interaction force can be measured by a load cell at the socket. We now show how to model the rocker foot in the context of equation (1) for the stance period.

Stance Period. During stance the COP is defined at the origin of the global reference frame. We model the rocker foot by constraining the heel point (x, y) to an arc that has radius R_f and intersects the COP (Fig. 1). The center of rotation P_f is defined in a moving reference frame such that the vector between P_f and the COP is always normal to the ground with radius $||P_f - COP|| = R_f$. This constraint is given in model coordinates by the equation $a_1^{\text{roll}}(q) = 0$ for

$$a_1^{\text{roll}}(q) := (x - R_f \sin(\phi))^2 + (y + R_f \cos(\phi))^2 - R_f^2. \quad (2)$$

We also constrain the foot orientation ϕ so the heel is perpendicular to the rocker, where the equation for the chord length between the heel and COP yields $a_2^{\text{roll}}(q) = 0$ for

$$a_2^{\text{roll}}(q) \;:=\; \phi - \gamma - 2\arcsin\left(\frac{\sqrt{x^2+y^2}}{2R_f}\right) \qquad (3)$$

on a ground slope of angle γ.

The foot does not go behind the heel, so depending on orientation ϕ the rocker may not be in contact with the ground at heel strike ($x = y = 0$). In this case the biped rotates about the heel using constraints $a_1^{\text{heel}}(q) := x$, $a_2^{\text{heel}}(q) := y$, which fix the heel position to the ground (i.e., acting as a point foot). The model switches to the rocker constraints (2)-(3) when the sole intersects the ground, i.e., when $a_2^{\text{roll}}(q) = 0$. We will discuss this transition in greater detail when modeling the full biped in Section IV.

Given either of these contact conditions, we follow the method in [14], [16] to compute the constraint matrix $A = \nabla_q a$ and Lagrange multiplier $\lambda = \widehat{\lambda} + \widetilde{\lambda}u + \bar{\lambda}F$, where

$$\widehat{\lambda} = W(\dot{A}\dot{q} - AM^{-1}(C\dot{q} + N)), \qquad (4)$$
$$\widetilde{\lambda} = WAM^{-1}B, \quad \bar{\lambda} = WAM^{-1}J^T$$

for $W = (AM^{-1}A^T)^{-1}$. We denote the heel contact matrix as A_{heel} and the rolling contact matrix as A_{roll}. Recall that the rocking constraints pertain only to the foot, whereas the effective shapes in Section III will characterize the pendular trajectory of the entire stance leg.

Swing Period. During the swing period, (x, y) is the heel point of the swing foot with respect to the global reference frame. The heel moves based on both the leg's own dynamics and interaction forces acting at the top of the leg. The COP is ill-defined for the swing foot, so we do not invoke the contact constraints, i.e., $A = 0$, $\lambda = 0$ in dynamics (1).

Since the prosthetic leg does not bear the user's body weight during the swing period, its joints can be accurately

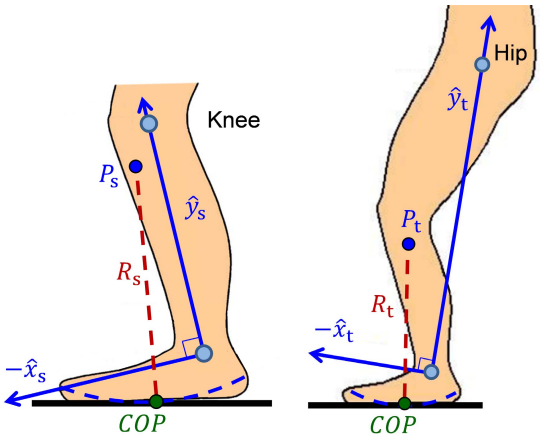

Fig. 2. Diagrams of the ankle-foot (left) and knee-ankle-foot (right) effective shapes. The COP moves along each shape (dashed curve) in the shank-based or thigh-based coordinate frame (solid axes).

controlled using traditional methods such as PD control. The swing knee and ankle primarily facilitate ground clearance during human locomotion, although these joints also have a role in step placement. In this paper we are interested in the challenging problem of stance-period control, so we simply implement PD control to drive the swing ankle to zero and the swing knee to a flexion angle of 0.4 rad:

$$u_{\rm sw}(\theta_{\rm a},\theta_{\rm k},\dot{\theta}_{\rm a},\dot{\theta}_{\rm k}) \;:=\; \begin{pmatrix} -k_{\rm pa}\theta_{\rm a} - k_{\rm da}\dot{\theta}_{\rm a} \\ -k_{\rm pk}(\theta_{\rm k}-0.3) - k_{\rm dk}\dot{\theta}_{\rm k} \end{pmatrix}. \quad (5)$$

We now use the leg model to derive the stance-period controller based on the human effective shape.

III. Effective Shape Control

We wish to design a prosthetic control system that mimics the effective shape of the biological leg during various locomotor tasks [12]. This shape characterizes how the ankle and knee move as the COP travels from heel to toe. We now derive the kinematic constraints for the AF and KAF shapes, which we will later enforce with a feedback controller.

Kinematic Constraints. The AF effective shape is the COP trajectory mapped into a shank-based reference frame (axes $\hat{x}_{\rm s}$, $\hat{y}_{\rm s}$ in Fig. 2, left). Able-bodied humans have effective shapes specific to activities such as walking or stationary swaying [12], and each shape can be characterized by the curvature of the COP trajectory with respect to a point $P_{\rm s} = (X_{\rm s}, Y_{\rm s})^T$ attached to the shank reference frame (Fig. 2). This can be expressed as the coordinate-free distance relationship

$$||P_{\rm s} - COP|| \;=\; R_{\rm s}(COP), \quad (6)$$

where the radius of curvature $R_{\rm s}$ is a function of the COP.

In the COP reference frame the effective center of rotation is given by the function

$$P_{\rm s}^{COP}(q) = (x,y)^T + \ell_{\rm f}(-\sin(\phi),\cos(\phi))^T + S(\rho)P_{\rm s} \quad (7)$$

where S is the standard rotation matrix parameterized by angle $\rho = \phi + \theta_{\rm a}$. Equation (6) is then given in our model coordinates by the kinematic constraint $h_{\rm s}(q) = 0$ for

$$h_{\rm s}(q) \;:=\; {\rm norm}(P_{\rm s}^{COP}(q))^2 - R_{\rm s}^2(x,y). \quad (8)$$

The KAF effective shape is the COP trajectory transformed into a thigh-based coordinate frame (axes $\hat{x}_{\rm t}$, $\hat{y}_{\rm t}$ in Fig. 2, right). This coordinate frame shares an origin with that of the AF effective shape, but the $y_{\rm t}$-axis is attached to the thigh at the hip joint. Defining a point $P_{\rm t} = (X_{\rm t}, Y_{\rm t})^T$ in this reference frame, the COP moves about $P_{\rm t}$ with radius of curvature $R_{\rm t}(COP)$. Therefore, the KAF effective shape is characterized by the distance relationship (6) with center of rotation $P_{\rm t}$ and curvature function $R_{\rm t}$. The KAF center of rotation is given in the COP reference frame by the function $P_{\rm t}^{COP}(q)$, which has the form (7) with rotation angle

$$\rho \;=\; \phi + \arctan\Big(\frac{\ell_{\rm s}\sin(\theta_{\rm a}) + \ell_{\rm t}\sin(\theta_{\rm a}+\theta_{\rm k})}{\ell_{\rm s}\cos(\theta_{\rm a}) + \ell_{\rm t}\cos(\theta_{\rm a}+\theta_{\rm k})}\Big).$$

Finally, the kinematic constraint for the KAF effective shape is given in our model coordinates by $h_{\rm t}(q) = 0$, where $h_{\rm t}$ is given by (8) in terms of $P_{\rm t}^{COP}$ and $R_{\rm t}$.

Both the AF and KAF constraints depend on the COP, which moves monotonically from heel to toe during steady walking. Therefore, a controller that virtually enforces these constraints will synchronize knee and ankle movement through mutual dependence on the COP as a phase variable.

Virtual Constraint Controller. We cannot expect to have either a model of the human or sensors at intact joints in a clinically viable system. The controller should then only rely on the prosthesis model and feedback available to onboard sensors, i.e., state $z = (q^T, \dot{q}^T)^T$ and interaction force F.

The coupled dynamics (1) of the weight-bearing prosthesis can be given in a modified control-affine form (cf. [17]):

$$\dot{z} = f(z) + g(z)u + j(z)F, \quad (9)$$

where the vector fields are defined as

$$f(z) = \begin{pmatrix} \dot{q} \\ -M(q)^{-1}\left(C(q,\dot{q})\dot{q} + N(q) + A^T(q)\lambda\right) \end{pmatrix}, \quad (10)$$
$$g(z) = \begin{pmatrix} 0_{5\times 5} \\ M^{-1}(q)B \end{pmatrix},\; j(z) = \begin{pmatrix} 0_{5\times 5} \\ M^{-1}(q)J^T(q) \end{pmatrix}.$$

Letting vector output $\xi := h(z) = (h_{\rm s}(z), h_{\rm t}(z))^T$, our goal is to define a feedback control law for u that drives ξ to zero in system (9). We first examine the output dynamics of the above system:

$$\dot{\xi} \;=\; (\nabla_z h)\dot{z} \;=\; L_f h + (L_g h)u + (L_j h)F, \quad (11)$$

where the Lie derivative $L_f h := (\nabla_z h)f$ characterizes the change of h along flows of vector field f [17], and it is easily shown that $L_g h = 0$ and $L_j h = 0$ for all z. Noting that no acceleration or control terms appear in $L_f h$, output ξ has relative degree greater than one (cf. [17]) and we must take another time-derivative to expose the control input u:

$$\ddot{\xi} \;=\; L_f^2 h + (L_g L_f h)u + (L_j L_f h)F. \quad (12)$$

Because the Lagrange multiplier defined in (4) explicitly depends on the external joint torques, so does the second Lie derivative $L_f^2 h = \widehat{L_f^2 h} + (\widehat{L_f^2 h})u + (\widehat{L_f^2 h})F$, where

$$\widehat{L_f^2 h} = (\nabla_q L_f h)\dot{q} - (\nabla_{\dot{q}} L_f h)M^{-1}(C\dot{q} + N + A^T\widehat{\lambda}),$$
$$\widetilde{L_f^2 h} = -(\nabla_{\dot{q}} L_f h)M^{-1}A^T\widetilde{\lambda},\; \overline{L_f^2 h} = -(\nabla_{\dot{q}} L_f h)M^{-1}A^T\bar{\lambda}.$$

Grouping the control input terms from (12), we can solve for the control law that inverts the output dynamics:

$$u_{\rm st}(z) \;:=\; D^{-1}(-\widehat{L_f^2 h} - (\overline{L_f^2 h} + L_j L_f h)F + v), \quad (13)$$

where the decoupling matrix $D = L_g L_f h + \widetilde{L_f^2 h}$ depends on q and is non-singular for feasible walking configurations. We then choose auxiliary input v to render the output dynamics linear and exponentially stable:

$$\ddot{\xi} \;=\; v \;:= -\begin{pmatrix} K_{\rm ps} & 0 \\ 0 & K_{\rm pt} \end{pmatrix}\xi - \begin{pmatrix} K_{\rm ds} & 0 \\ 0 & K_{\rm dt} \end{pmatrix}\dot{\xi} \quad (14)$$

with positive PD gains. Given sensor measurements of z and F and actuation of u, (14) implies $\xi(t) \to 0$ exponentially fast as $t \to \infty$ for $\xi(0) \neq 0$. The PD terms will correct errors resulting from perturbations such as discontinuous impact events, which we will see when modeling the full biped next.

IV. Simulation Results

Now that we have designed a controller for the prosthetic leg, we wish to study it during simulated walking with the full biped model of Fig. 1. This requires us to consider the coupled dynamics of the body and the controlled prosthesis. We can approximate the behavior of the human-in-the-loop by exploiting the existence of passive walking gaits. Passive gaits arise on declined surfaces when the potential energy converted into kinetic energy during each step period replenishes the energy dissipated at impact events [18], [19]. This behavior reflects certain characteristics of human walking, such as ballistic swing motion [20] and energetic efficiency down slopes [21]. We have already modeled the swing period of the prosthetic leg to behave passively, and we will do the same with the hip joint of the body.

Biped Model. For simplicity we assume each leg employs controller (13) during stance and controller (5) during swing (as in the case of a bilateral amputee). The legs do not communicate, so each prosthesis interacts with the hip and opposing leg in (1) as it would with the human body.

The configuration vector of the full biped is denoted by $\breve{q} = (q^T, \theta_{\rm h}, \theta_{\rm sa}, \theta_{\rm sk})^T$, where $\theta_{\rm h}$ is the body's hip angle, $\theta_{\rm sa}$ is the swing ankle angle, and $\theta_{\rm sk}$ is the swing knee angle. After heel strike the biped's dynamics are governed by a differential equation of the form (1), using heel contact constraint matrix $\breve{A}_{\rm heel} = \nabla_{\breve{q}} a^{\rm heel}$ until the foot sole intersects the ground when $a_2^{\rm roll}(\breve{q}) = 0$. The subsequent foot slap is modeled as an instantaneous impact, where the joint velocities change to $\dot{\breve{q}}^+ = \dot{\breve{q}}^- - \mathcal{X}(\breve{A}_{\rm roll}\mathcal{X})^{-1}\breve{A}_{\rm roll}\dot{\breve{q}}^-$ with $\mathcal{X} = \breve{M}^{-1}\breve{A}_{\rm roll}^T$, satisfying the rolling contact constraints provided by $\dot{A}_{\rm roll} = \nabla_{\breve{q}} a^{\rm roll}$ (cf. [19], superscripts $+/-$ respectively denote post/pre-impact).

The dynamics are then simulated under rolling contact until the swing foot contacts the ground, which initiates the next step. We define a function $H_\gamma(\breve{q})$ to give the height of the heel of the swing foot above ground with slope angle γ. The subsequent double-support transition is modeled as an instantaneous impact event with a perfectly plastic (inelastic) collision as in [6]. The state trajectory is subjected to the discontinuous impact map Δ, which also changes the values of $\breve{q}$ to re-label the stance/swing legs. The dynamics for one step period are therefore given sequentially by

$$\begin{aligned}
\breve{M}(\breve{q})\ddot{\breve{q}} + \breve{C}(\breve{q},\dot{\breve{q}})\dot{\breve{q}} + \breve{N}(\breve{q}) + \breve{A}_{\rm heel}^T(\breve{q})\breve{\lambda} &= \breve{\tau}, && a_2^{\rm roll}(\breve{q}) \neq 0 \\
\dot{\breve{q}}^+ &= \dot{\breve{q}}^- - \mathcal{X}(\breve{A}_{\rm roll}\mathcal{X})^{-1}\breve{A}_{\rm roll}\dot{\breve{q}}^-, && a_2^{\rm roll}(\breve{q}) = 0 \\
\breve{M}(\breve{q})\ddot{\breve{q}} + \breve{C}(\breve{q},\dot{\breve{q}})\dot{\breve{q}} + \breve{N}(\breve{q}) + \breve{A}_{\rm roll}^T(\breve{q})\breve{\lambda} &= \breve{\tau}, && H_\gamma(\breve{q}) \neq 0 \\
(\breve{q}^+, \dot{\breve{q}}^+) &= \Delta(\breve{q}^-, \dot{\breve{q}}^-), && H_\gamma(\breve{q}) = 0
\end{aligned}$$

which then returns to the beginning of the sequence for the next step. Note that the accented terms for the full model are defined as in Section II, and all control torques are given by

$$\breve{\tau} = [B^T, 0_{2\times 3}]^T u_{\rm st} + [0_{1\times 5}, 1, 0_{1\times 2}]^T u_{\rm h} + [0_{2\times 6}, I_{2\times 2}]^T u_{\rm sw},$$

where we achieve more consistent step placement by augmenting the body's passive dynamics with the hip input $u_{\rm h}(\theta_{\rm h}, \dot{\theta}_{\rm h}) := -k_{\rm ph}(\theta_{\rm h} + 0.4) - k_{\rm dh}\dot{\theta}_{\rm h}$.

This biped model is known as a hybrid dynamical system. Letting $\breve{z} = (\breve{q}^T, \dot{\breve{q}}^T)^T$ be the state vector for the full biped, walking gaits are cyclic and correspond to solution curves $\breve{z}(t)$ of the hybrid system such that $\breve{z}(t) = \breve{z}(t+T)$ for all $t \geq 0$ and some minimal $T > 0$. These solutions define isolated orbits in state space known as *hybrid limit cycles*, which correspond to equilibria of the *Poincaré* map $P : G \to G$, where $G = \{\breve{z} \mid H_\gamma(\breve{q}) = 0\}$ is the switching surface indicating heel strike. This return map represents a hybrid system as a discrete system between impact events, sending state $\breve{z}_j \in G$ ahead one step to $\breve{z}_{j+1} = P(\breve{z}_j)$. A periodic solution $\breve{z}(t)$ then has a fixed point $\breve{z}^* = P(\breve{z}^*)$. We verify stability about $\breve{z}^*$ by approximating the linearized map $\nabla_{\breve{z}} P(\breve{z}^*)$ through a perturbation analysis [18]. The linearized discrete system is *exponentially stable* if the eigenvalues of $\nabla_{\breve{z}} P(\breve{z}^*)$ are within the unit circle, by which we can infer local stability of the hybrid limit cycle.

TABLE I
Model and Controller Parameters

Parameter	Variable	Value
Hip mass	$m_{\rm h}$	31.73 [kg]
Thigh mass	$m_{\rm t}$	9.45 [kg]
Thigh moment of inertia	$I_{\rm t}$	0.1995 [kg·m^2]
Thigh/shank length	$\ell_{\rm t}$, $\ell_{\rm s}$	0.428 [m]
Shank mass	$m_{\rm s}$	4.05 [kg]
Shank moment of inertia	$I_{\rm s}$	0.0369 [kg·m^2]
Heel height	$\ell_{\rm f}$	0.07 [m]
Foot mass	$m_{\rm f}$	1 [kg]
Foot radius	$R_{\rm f}$	0.257 [m]
Slope angle	γ	0.03 [rad]
KAF/AF effective radius	$R_{\rm t}$, $R_{\rm s}$	0.351 [m]
KAF/AF proportional gain	$K_{\rm pt}$, $K_{\rm ps}$	121.46 [N/m]
KAF/AF derivative gain	$K_{\rm dt}$, $K_{\rm ds}$	15.43 [N·s/m]
KAF center of rotation	$X_{\rm t}$	0 [m]
AF center of rotation	$X_{\rm s}$	0.015 [m]
Swing hip proportional gain	$k_{\rm ph}$	6.073 [Nm/rad]
Swing hip derivative gain	$k_{\rm dh}$	2.464 [Nm·s/rad]
Swing knee proportional gain	$k_{\rm pk}$	12.146 [Nm/rad]
Swing knee derivative gain	$k_{\rm dk}$	2.091 [Nm·s/rad]
Swing ankle proportional gain	$k_{\rm pa}$	121.46 [Nm/rad]
Swing ankle derivative gain	$k_{\rm da}$	15.43 [Nm·s/rad]

Simulations. The model parameters of Table I consist of average values from adult males reported in [22], with the

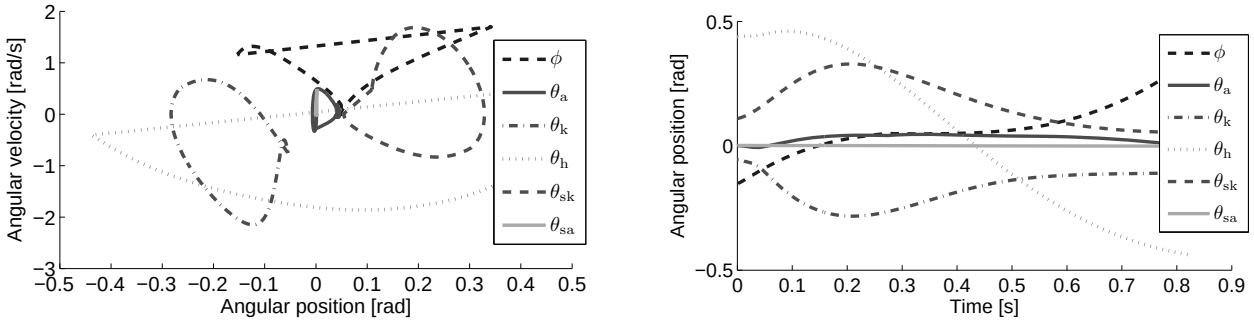

Fig. 3. Angular phase portrait (left) and angular time-trajectories (right) during steady-state walking.

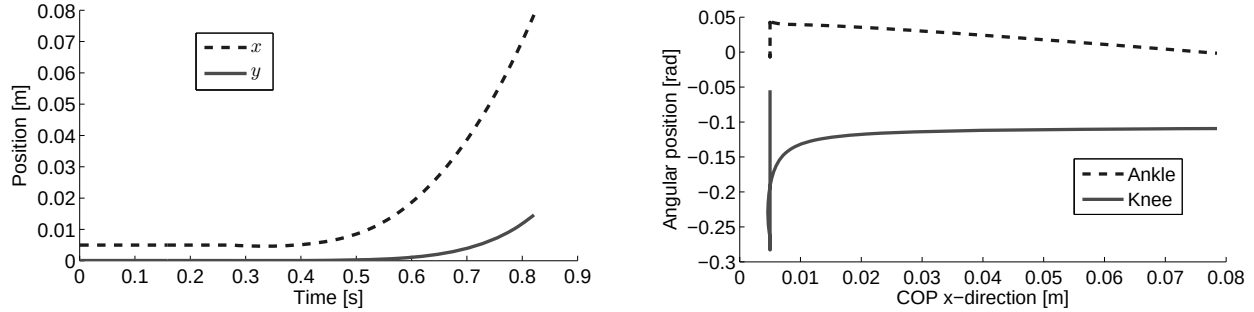

Fig. 4. COP over time (left) and stance ankle/knee over COP (right) during steady-state walking. Note that the foot initially contacts the ground 5 mm in front of the heel (positive x-direction) to avoid a singularity in the contact constraints.

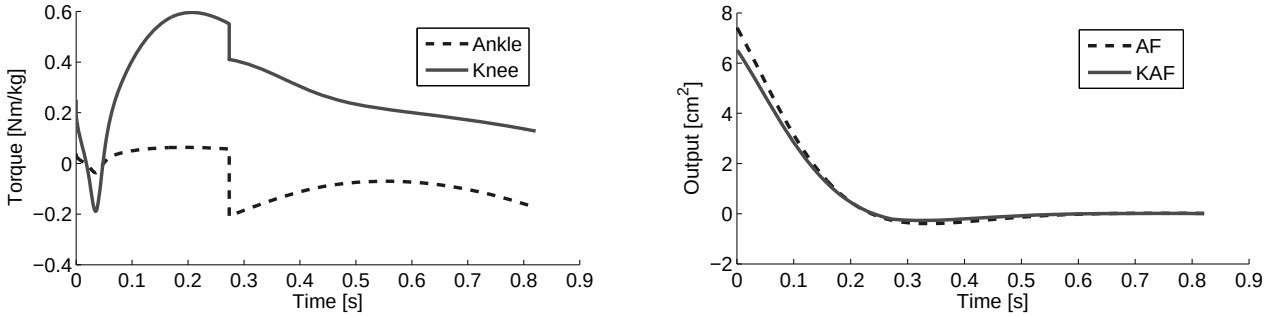

Fig. 5. Control torques (left) and outputs (right) over time during steady-state walking.

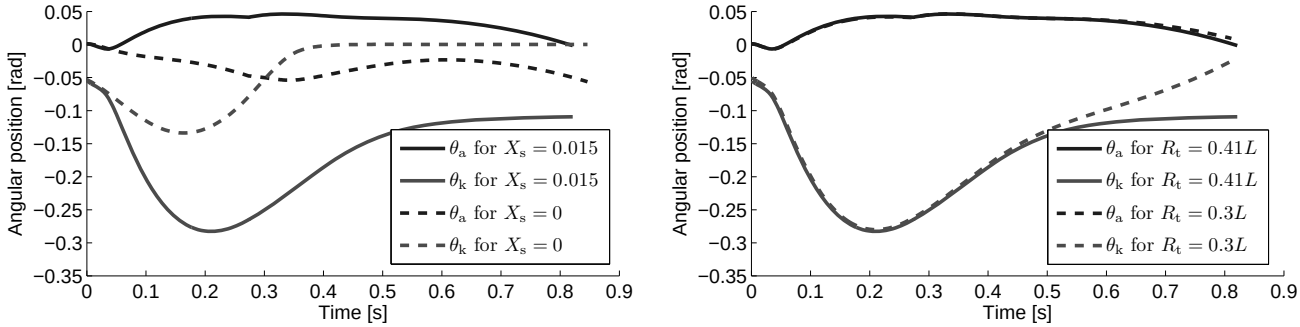

Fig. 6. Stance ankle and knee angles over time. Left: $X_{\mathrm{s}} = 0.015$ (solid) vs. $X_{\mathrm{s}} = 0$ (dashed). Right: $R_{\mathrm{t}} = 0.41L$ (solid) vs. $R_{\mathrm{t}} = 0.3L$ (dashed).

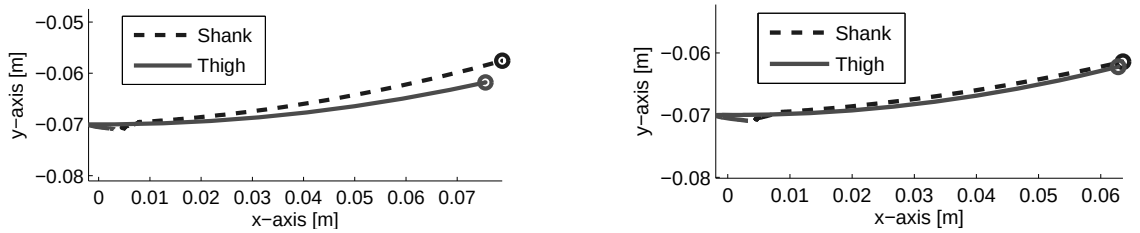

Fig. 7. Effective shapes with $R_{\mathrm{s}} = R_{\mathrm{t}} = 0.41L$ (left) and $R_{\mathrm{t}} = 0.3L$ (right) in shank-based (AF shape) or thigh-based (KAF shape) reference frame. Circles indicate contralateral heel strike. The AF and KAF shapes on the left are oriented differently due to their different centers of rotation.

trunk masses grouped at the hip. The physical foot radius is set to $R_{\rm f} = 0.3L$ for leg length $L = \ell_{\rm s} + \ell_{\rm t}$, which is characteristic of human foot compliance [15].

During walking the effective radius of curvature is constant for both the KAF and AF shapes (circular arcs in Fig. 2). Their radii were found to be approximately the same, $R_{\rm t} = R_{\rm s} = 0.41L$, in the studies of [9]. Humans have a plantarflexed KAF shape on downhill slopes [9], so Table I defines $X_{\rm s}$ slightly behind the shank and $X_{\rm t}$ at the hip for walking in the negative x-direction. The other component of $P_{\rm s}$ is given by $Y_{\rm s} = \sqrt{R_{\rm s}^2 - X_{\rm s}^2} - \ell_{\rm f}$ because condition (6) must be satisfied at the zero configuration, when the COP is co-linear with the shank. The two leg-based reference frames in Fig. 2 share an origin, so we also have $Y_{\rm t} = \sqrt{R_{\rm t}^2 - X_{\rm t}^2} - \ell_{\rm f}$. We choose $K_{\rm ps} = K_{\rm pt} = 2$ N/m/kg and $K_{\rm ds} = K_{\rm dt} = 2\zeta\sqrt{K_{\rm ps}}$ to achieve damping ratio $\zeta = 0.7$ in the linearized output dynamics (14).

The dynamics, interaction forces, and control law (13) are simultaneously computed from both the full biped model and the prosthesis model in *MATLAB*. Walking gaits are found for our choice of parameters using the methods in [18]. Once the biped has converged to a steady-state gait, we verify that the associated fixed point is locally exponentially stable, using the procedure in [18]. A supplemental video of the animated walking gait is available at `http://vimeo.com/49347309`.

The hybrid limit cycle is shown in the phase portrait and trajectories of Fig. 3 and 4. The biped has heel contact for 270 ms followed by rolling contact for 551 ms (Fig. 4). This contact transition causes a discontinuity in the torque trajectories of Fig. 5 (left), but controller (13) drives the outputs toward zero during both contact conditions. Every ground-strike event re-introduces a small amount of output error, but the outputs converge to zero within the step period (Fig. 5, right), implying both effective shapes are enforced.

The stance knee trajectory shown in Fig. 3 has human-like range-of-motion with up to 16.2 degrees of flexion after ipsilateral heel strike (compared to about 18 degrees in humans [13]). The KAF center of rotation was chosen less than the AF center to induce this knee flexion [9], which is especially important when walking downhill. We also see ankle plantarflexion at the end of the step period. Viewing these trajectories as a function of the COP—our phase variable—in Fig. 4 (right), we see nearly constant slopes during the majority of rolling contact.

We demonstrate the effect of the centers of rotation by setting $X_{\rm s}$ equal to $X_{\rm t} = 0$. The resulting trajectories of the stance ankle and knee are superimposed against the original trajectories in Fig. 6 (left). Moving the AF center closer to the shank has two consequences: the ankle is more plantarflexed and the knee is less flexed than before (in fact, the knee angle approaches zero). Desirable knee flexion can be retained if we also decrease $X_{\rm t}$, as the difference $X_{\rm s} - X_{\rm t}$ appears to determine the amount of knee motion. This relationship is to be expected since the KAF shape depends on the ankle, whereas the AF shape does not depend on the knee. Note that the change in $X_{\rm s}$ has little influence on the COP trajectory.

Although the choice $R_{\rm t} = R_{\rm s}$ approximates human data, it is possible to choose non-equal values. Fig. 6 (right) shows the stance ankle/knee trajectories after changing the KAF radius to $R_{\rm t} = 0.3L$. This causes little change in the ankle, and the knee trajectory only differs near the end of the step period with less flexion. The biped remains in heel contact longer and the COP range-of-motion decreases by almost 2 cm, which we see in the effective shapes of Fig. 7. We previously reported in [14] that walking speed, step length, step period, and COP motion increase with a larger AF radius, and this trend also appears true with the KAF shape.

V. Discussion

The proposed control strategy can potentially improve the clinical viability of powered prostheses. This knee-ankle control strategy requires tuning of only five independent control parameters ($R_{\rm s} = R_{\rm t}$, $K_{\rm ps} = K_{\rm pt}$, $K_{\rm ds} = K_{\rm dt}$, $X_{\rm s}$, $X_{\rm t}$) for the entire single-support period, whereas other control approaches have many more parameters during stance (e.g., 18 for event-based impedance control [3], 14 for the muscle model of one joint [4], or an entire look-up table for tracking human data [5]). We chose the same PD gains for both shapes so their respective outputs would have the same rate of convergence by virtue of the linearization (Fig. 5). The effective radius $R_{\rm s} = R_{\rm t}$ is a fraction of the user's leg length and the rotational centers $X_{\rm s}$, $X_{\rm t}$ respectively determine the amount of flexion in the ankle/knee joints, offering a simple tuning procedure. Moreover, the output linearization approach can accurately enforce constraints with much smaller gains than standard PD control [7], which is desirable for stability in the presence of feedback time delay and for safety when interacting with humans.

We also showed that output linearization can be achieved on a prosthetic leg using measurements of interaction forces in place of state feedback from the human body. Load cells are common in modern prosthetic legs (e.g., [3], [4]) and can also be used to measure the COP [23]. Our controller depends on the global foot orientation ϕ, which can be measured with a rate gyro and filtered as done in [5]. The controller does not require the slope angle γ because matrix $A_{\rm roll}$ consists of partial derivatives of (3), which eliminate any dependence on γ. The matrix $A_{\rm roll}$ does, however, depend on the radius of foot compliance $R_{\rm f}$, which has already been characterized for many prosthetic feet in [11].

The walking model used to simulate our controller has limitations, including its COP motion, instantaneous double-support period, and downhill slope. Our first gait has no COP motion until 270 ms into the stance period, whereas humans have strictly monotonic COP trajectories during steady walking [13]. The COP does not represent the gait cycle phase of our model during heel contact (note the hysteresis in Fig. 4, right), so a more human-like COP trajectory would make our controller an even better match for human behavior (as seen in the preliminary experiments of [23]). Moreover, the controller would not need to switch its contact constraint, as real feet comply continuously during stance (i.e., the foot never has true point contact).

A non-trivial double-support period could be modeled using a compliant ground contact model, which has been done in the context of output linearization [24]. However, the constant-curvature property of the effective shape does not hold after contralateral heel strike [9]. The main challenge is then to extend the kinematic model of the effective shape into the double-support period (and possibly the swing period), e.g., by using the theoretical COP of the support polygon, which can be located between the two feet.

By relying on passive dynamics to generate the body's joint patterns, we were limited to testing our controller with a downhill walking task. We can mimic human behavior on different slopes by rotating the effective centers of rotation P_s, P_t by the slope change [9]. Stationary fore-aft swaying also has a constant effective radius—about six times that of a walking task [12]. The output functions h_s, h_t allow the radii of curvature R_s, R_t to be functions of the COP, which may be the case for tasks like stair climbing.

VI. Conclusion

We showed that the effective shapes between the COP, ankle, and knee correspond to two kinematic constraints, which can be enforced as virtual constraints by an output linearizing control law using only feedback available to sensors onboard a prosthetic leg. Therefore knee and ankle control during walking can be coordinated by one simple objective: maintaining constant curvature in the effective shapes. Due to shape invariance over walking speeds, body weights, and heel heights [9], this choice of constraints allows the prosthesis to naturally adapt to the user. The constraints can also be systematically tuned to produce the effective shapes corresponding to different activities, e.g., standing and stair climbing, by changing the center of rotation or curvature function for each shape.

Preliminary experiments with our controller are presented in [23]. Future work could integrate our controller with a neural interface (e.g., using electromyography from residual muscles [25]) to allow the user to subconsciously adapt the effective shapes when anticipating a task change.

Our control approach can possibly be extended into three dimensions by investigating the effective shape of mediolateral motion during walking. Our formulation of output linearization for prosthetics can also enforce other kinematic constraints unrelated to effective shape. This framework motivates investigation of a general control theory for wearable robots, including powered orthoses [26], [27].

Acknowledgments

We thank Andrew Hansen for discussions on his studies.

References

[1] W. Miller, A. Deathe, M. Speechley, and J. Koval, "The influence of falling, fear of falling, and balance confidence on prosthetic mobility and social activity among individuals with a lower extremity amputation," *Arch. Phys. Med. & Rehab.*, vol. 82, no. 9, pp. 1238–1244, 2001.

[2] R. S. Gailey, M. A. Wenger, M. Raya, N. Kirk, K. Erbs, P. Spyropoulos, and M. S. Nash, "Energy expenditure of trans-tibial amputees during ambulation at self-selected pace," *Prosthetics & Orthotics Int.*, vol. 18, no. 2, p. 84, 1994.

[3] F. Sup, H. Varol, and M. Goldfarb, "Upslope walking with a powered knee and ankle prosthesis: Initial results with an amputee subject," *IEEE Trans. Neural Systems & Rehab. Eng.*, vol. 19, no. 1, pp. 71–78, 2011.

[4] M. Eilenberg, H. Geyer, and H. Herr, "Control of a powered ankle–foot prosthesis based on a neuromuscular model," *IEEE Trans. Neural Systems & Rehab. Eng.*, vol. 18, no. 2, pp. 164–173, 2010.

[5] M. A. Holgate, T. G. Sugar, and A. W. Bohler, "A novel control algorithm for wearable robotics using phase plane invariants," in *IEEE Int. Conf. Robotics & Automation*, 2009, pp. 3845–3850.

[6] E. R. Westervelt, J. W. Grizzle, C. Chevallereau, J. H. Choi, and B. Morris, *Feedback Control of Dynamic Bipedal Robot Locomotion*. New York, NY: CRC Press, 2007.

[7] K. Sreenath, H. W. Park, I. Poulakakis, and J. W. Grizzle, "A compliant hybrid zero dynamics controller for stable, efficient and fast bipedal walking on MABEL," *Int. J. Robotics Res.*, vol. 30, no. 9, pp. 1170–1193, 2011.

[8] R. D. Gregg and L. Righetti, "Controlled reduction with unactuated cyclic variables: Application to 3D bipedal walking with passive yaw rotation," *IEEE Trans. Automatic Control*, 2013, in press.

[9] A. Hansen and D. Childress, "Investigations of roll-over shape: Implications for design, alignment, and evaluation of ankle-foot prostheses and orthoses," *Disability & Rehab.*, vol. 32, no. 26, pp. 2201–2209, 2010.

[10] A. Hansen, D. Childress, and E. Knox, "Roll-over shapes of human locomotor systems: Effects of walking speed," *Clinical Biomechanics*, vol. 19, no. 4, pp. 407–414, 2004.

[11] A. Hansen and D. Childress, "Effects of shoe heel height on biologic rollover characteristics during walking," *J. Rehab. Res. & Dev.*, vol. 41, no. 4, pp. 547–554, 2004.

[12] A. Hansen and C. Wang, "Effective rocker shapes used by able-bodied persons for walking and fore-aft swaying: Implications for design of ankle-foot prostheses," *Gait & Posture*, vol. 32, no. 2, pp. 181–184, 2010.

[13] J. Rose and J. Gamble, *Human Walking*, 3rd ed. New York, NY: Lippincott Williams & Wilkins, 2006.

[14] R. D. Gregg and J. W. Sensinger, "Towards biomimetic virtual constraint control of a powered prosthetic leg," *IEEE Trans. Control Sys. Tech.*, 2013, in press.

[15] P. G. Adamczyk, S. H. Collins, and A. D. Kuo, "The advantages of a rolling foot in human walking," *J. Exp. Biology*, vol. 209, no. 20, p. 3953, 2006.

[16] R. M. Murray, Z. Li, and S. S. Sastry, *A Mathematical Introduction to Robotic Manipulation*. Boca Raton, FL: CRC Press, 1994.

[17] S. S. Sastry, *Nonlinear Systems: Analysis, Stability and Control*. New York, NY: Springer-Verlag, 1999.

[18] R. D. Gregg, Y. Y. Dhaher, A. Degani, and K. M. Lynch, "On the mechanics of functional asymmetry in bipedal walking," *IEEE Trans. Biomed. Eng.*, vol. 59, no. 5, pp. 1310–1318, 2012.

[19] F. Asano and M. Yamakita, "Extended PVFC with variable velocity fields for kneed biped," in *IEEE Int. Conf. Human. Rob.*, 2000.

[20] S. Mochon and T. A. McMahon, "Ballistic walking," *J. Biomechanics*, vol. 13, no. 1, pp. 49–57, 1980.

[21] A. Minetti, C. Moia, G. Roi, D. Susta, and G. Ferretti, "Energy cost of walking and running at extreme uphill and downhill slopes," *J. Applied Physiology*, vol. 93, no. 3, pp. 1039–1046, 2002.

[22] P. De Leva, "Adjustments to Zatsiorsky-Seluyanov's segment inertia parameters," *J. Biomechanics*, vol. 29, no. 9, pp. 1223–1230, 1996.

[23] R. D. Gregg, T. Lenzi, N. P. Fey, L. J. Hargrove, and J. W. Sensinger, "Experimental effective shape control of a powered transfemoral prosthesis," in *IEEE Int. Conf. Rehab. Robotics*, Seattle, WA, 2013.

[24] M. Scheint, M. Sobotka, and M. Buss, "Virtual holonomic constraint approach for planar bipedal walking robots extended to double support," in *IEEE Conf. Decision & Control*, Shanghai, China, 2009, pp. 8180–8185.

[25] L. Hargrove, A. Simon, R. Lipschutz, S. Finucane, and T. Kuiken, "Real-time myoelectric control of knee and ankle motions for transfemoral amputees," *J. Amer. Med. Assoc.*, vol. 305, no. 15, pp. 1542–1544, 2011.

[26] R. D. Gregg, T. W. Bretl, and M. W. Spong, "A control theoretic approach to robot-assisted locomotor therapy," in *IEEE Conf. Decision and Control*, Atlanta, GA, 2010, pp. 1679–1686.

[27] K. A. Shorter, E. T. Hsiao-Wecksler, G. F. Kogler, E. Loth, and W. K. Durfee, "A portable powered ankle-foot-orthosis for rehabilitation," *J. NeuroEng. & Rehab.*, vol. 48, no. 4, pp. 459–472, 2011.